Femtosecond velocity map imaging of concerted photodynamics in CF2I2

Roeterdink, W.; Janssen, M.H.M.

published in
Journal of Chemical Physics
2002

DOI (link to publisher)
10.1063/1.1505026

document version
Publisher's PDF, also known as Version of record

Femtosecond velocity map imaging of concerted photodynamics in CF_2I_2

Wim G. Roeterdink and Maurice H. M. Janssen[a)]
Laser Centre and Department of Chemistry, Vrije Universiteit, de Boelelaan 1083, 1081 HV Amsterdam, The Netherlands

(Received 21 February 2002; accepted 16 July 2002)

The femtosecond pump–probe technique is used in combination with velocity map ion imaging to study the photodissociation dynamics of CF_2I_2. Velocity map ion imaging provides the kinetic energy and the angular recoil distribution of the detected fragments. It enables us to distinguish between multiple photoexcitation and dissociation pathways leading to the same ionic fragment. For the dissociation of CF_2I_2 with delayed femtosecond pulses at 264 and 396 nm, various ionic fragments and dissociation channels are observed. Especially interesting dynamics is observed for the molecular detachment of I_2. It is found that at short pump–probe delay ($\leqslant$250 fs) I_2^+ can be formed via a one-photon excitation at 264 nm and subsequent ionization of the dissociating neutral CF_2I_2 molecule. This excitation pathway produces slow I_2^+ fragments recoiling predominantly parallel along the polarization of the 264 nm pump laser. At long delay time ($\geqslant$500 fs) this pathway is closed and the formation of molecular I_2^+ proceeds via a two-photon excitation at 264 nm to a highly electronically excited state of the CF_2I_2 molecule. The molecular detachment of I_2 is via a concerted asynchronous dissociation producing a highly internally excited I_2^* fragment, possibly in the $^2\Pi_{3/2}5d;2g$ state. The highly excited I_2 fragments are ionized by a single 396 nm photon producing I_2^+ fragments. The kinetic energy of this pathway is higher and the I_2^+ fragments are recoiling perpendicular with respect to the polarization of the pump laser. © *2002 American Institute of Physics.* [DOI: 10.1063/1.1505026]

I. INTRODUCTION

The molecular detachment of halogenated alkanes has been studied intensively over the last few years using various techniques. One of the foci of the studies has been the detailed reaction mechanism leading to the formation of a molecular fragment. Molecular detachment reactions are of special interest because they are the reverse reactions of the attack of a carbene on a molecule with a sigma bond.[1] Reactions with CF_2 are of special interest in organic chemistry and in atmospheric chemistry. Much work has been done on CF_2 reactions with molecules like O_2, Cl_2, and Br_2.[2]

The advances in femtosecond chemistry over the last decade[3] makes it possible to study the mechanism of molecular detachment, e.g., a concerted bondbreaking process versus a sequential process, on the time scale of the event.

Dantus and co-workers reported on the detachment of various Y_2 and YZ molecular fragments from multiphoton dissociation of CX_2YZ (where X=H, F or Cl and Y, Z=I, Br or Cl) using femtosecond time-resolved techniques with fluorescence depletion detection of the electronically excited molecular fragment.[4,5] They concluded that the low rotational excitation observed for the heteronuclear YZ fragments was due to a symmetry allowed synchronous concerted elimination, whereas for the homonuclear Y_2 fragments, a symmetry barrier resulted in an asynchronous bondbreaking process with high rotational excitation like in the multiphoton dissociation of CH_2I_2.[4]

Radloff and co-workers studied the photon-induced dissociation dynamics of CF_2I_2 using time-resolved photoion–photoelectron coincidence detection.[6] The dissociation of CF_2I_2 has different fragmentation channels depending on the photon excitation and whether the process is a single photon absorption or a multiphoton absorption (Fig. 1). CF_2I_2 can decay following a three-body fragmentation in the form of CF_2+I+I, or the parent molecule can eliminate molecular iodine. In the latter two-body fragmentation the process of breaking the two C–I bonds can be either sequential or concerted. Ion detection of dissociation dynamics in combination with femtosecond laser techniques allows for the additional information on the mass of the species produced, as was first demonstrated using femtosecond pump–probe spectroscopy for methyl iodide multiphoton induced Rydberg state dynamics.[7] For the CF_2I_2 molecule, the combination of photoelectron detection in coincidence with ion time-of-flight (TOF) detection makes it possible to distinguish the various multiphoton induced fragmentation pathways leading to the formation of atomic and molecular ionic fragments. Radloff and co-workers concluded that in the one photon dissociation at 267 nm three different electronic surfaces play a role, with ultrafast internal conversion between the electronic states. The dominant channel for the various ionic species is ionization and fragmentation by the probe pulse at 400 nm from two of these electronically excited states. A

a)Author to whom correspondence should be addressed. Electronic mail: mhmj@chem.vu.nl; Fax: +31(0)20 4447643.

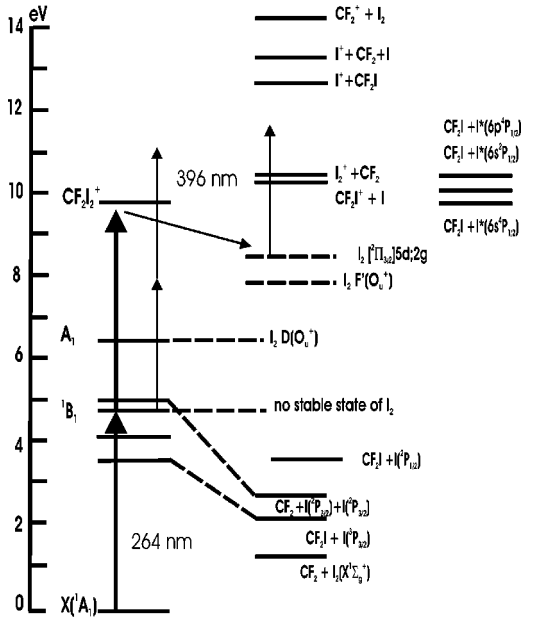

FIG. 1. Level scheme of CF_2I_2 adapted from Ref. 6, which includes the relevant energy levels for our excitation wavelengths. Note that we used the symmetry assignment for the bands around 4–5 eV of Ref. 10, which differs from the recent theoretical assignment of Ref. 12.

minor channel is attributed to multiphoton absorption of the pump pulse.[6]

The photodynamics of CF_2I_2 has been extensively studied by Huber and co-workers[8–11] using nanosecond laser techniques in combination with neutral fragment time-of-flight with electron impact and quadrupole mass detection. At 248 nm excitation wavelength a concerted three body decay was observed, whereas at wavelengths above 308 nm only the process $CF_2I_2 \rightarrow CF_2I + I(^2P_{1/2}, ^2P_{3/2})$ was observed. From polarization measurements they concluded that the electronic state excited around 248 nm has $^1B_1$ symmetry, using the C_{2v} group symmetry labels.[10] The primary bondbreaking process was found to be on the subpicosecond time scale. At these excitation wavelengths, 248–308 nm, the formation of molecular iodine was never observed using nanosecond pulsed laser excitation. Huber and co-workers attributed this to the fact that dynamics from the $^1B_1$ surface does not correlate with stable and energetically accessible states of I_2. In other photodissociation experiments at 193 nm they observed the formation of molecular iodine with high internal energy, possibly even in electronically excited states.[11] However, recent density functional theoretical calculations of the ultraviolet excited electronic states of CF_2I_2 assign the band at 248 nm to a state of $^1A_1$ symmetry and the band at 267 nm to $^1A_2$ and $^1B_2$ excitations.[12] This appears to be in contrast with the conclusions from the experimental studies at 248 nm by Huber and co-workers. The same absorption band in CF_2Br_2 studied at 234 and 267 nm, does form Br_2 and is assigned to be of $^1B_1$ symmetry.[13] The formation of Br_2 was attributed to an avoided crossing with a state of $^1A_1$ symmetry.

In this paper we report on femtosecond time-resolved velocity map ion imaging experiments of CF_2I_2. The application of ion imaging[14] for the study of chemical reaction dynamics enables the complete measurement of kinetic and angular distributions of photofragments. We have recently combined the improved technique of velocity mapping[15] with femtosecond spectroscopy to study the multiphoton induced dynamics in CF_3I.[16,17] In Sec. II we will give a brief description of the experimental setup. In Sec. III we present the femtosecond transients and images observed from excitation with femtosecond pulses at 264 and 396 nm. In Sec. IV we discuss the kinetic and angular distributions of the various ionic fragments and the dissociation mechanism responsible for the particular channels. Finally, we will summarize our conclusions in Sec. V.

II. EXPERIMENT

The experimental setup has been described in full detail recently,[17] therefore we will only give a brief description here. The CF_2I_2 molecules (Fluorchem) were seeded (0.1%) in Ar and cooled by expansion through a pulsed nozzle operating at 1 kHz. After passing two skimmers, which bound the differentially pumped buffer chamber, the molecular beam enters the ionization chamber. In this third chamber the molecular beam is intersected by two collinearly propagating femtosecond laser pulses at a position in the middle between the repellor and extractor plates of a set of ion lenses. The ion optics are designed to map the velocity of the produced ionized fragments on a mass-gated the microchannel-plate (MCP) detector, 36 cm downstream of the ionization region. The intensities of the pump and probe laser beams were chosen such that about 10 parent ions per laser shot were formed when the pump and probe pulses were overlapped in time. The femtosecond chirped-regen laser system was running at 1 kHz. The pulse energies were about 2 μJ for the pump laser (264 nm) and 20 μJ for the probe laser (396 nm). The waists of both laser beams were measured with calibrated pinholes to be about 200 μm diam. Care was taken that the foci of the laser beams were behind the intersection point with the molecular beam. This gives an upper limit to the fluences of 6 mJ/cm^2 for the pump and 60 mJ/cm^2 for the probe. The electrons emitted from the MCP plates are accelerated toward a phosphor screen. The phosphorescence is imaged with a sensitive slow scan CCD camera, and simultaneously by a photomultiplier for total ion yield. Images were taken at various delay times between pump and probe pulses. To account for background and one-laser contributions images were measured with both laser pulses entering the ionization region, as well as images with pump and probe beams separately. The data treatment was described previously.[17]

III. RESULTS

A. Transients

In the time-of-flight spectrum five ion-peaks are observed corresponding to the fragments CF_2^+, I^+, CF_2I^+, I_2^+, and $CF_2I_2^+$. The transients measured on each ion peak are shown in Fig. 2. These transients show either an enhancement at the right-hand side or at the left-hand side of the $\tau=0$ spike. The sign of the time delay is defined as follows: If the 396 nm pulse is after the 264 nm pulse the delay time is

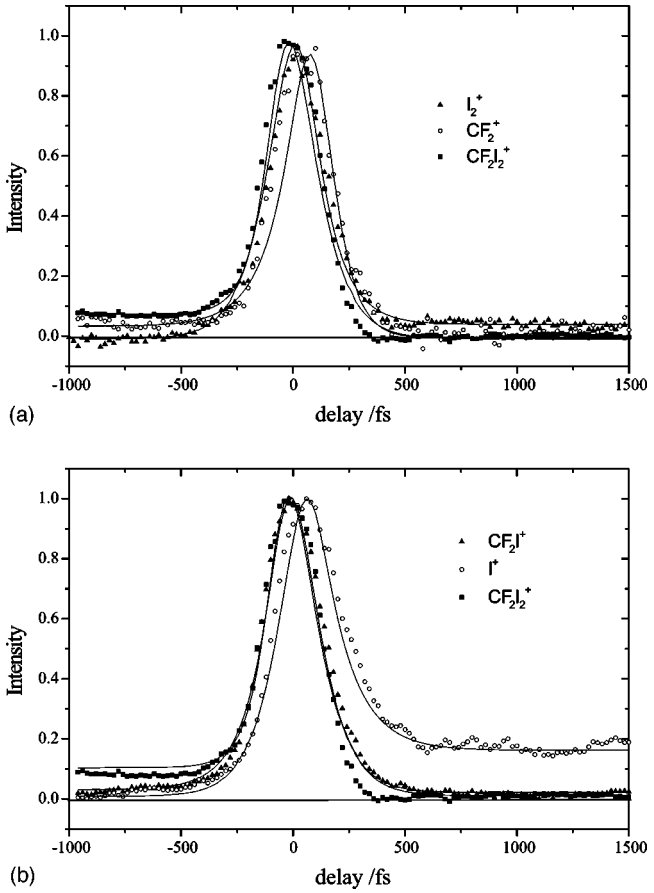

FIG. 2. (a) Pump–probe transients of the fragments I_2^+, CF_2^+, and $CF_2I_2^+$, at relatively high laser intensities of 6 mJ/cm^2 (264 nm) and 60 mJ/cm^2 (396 nm). These fluences produce about 10 I_2^+ ions per laser shot. Note that all transients are normalized to their maximum value. (b) Pump–probe transients of the fragments CF_2I^+, I^+, and $CF_2I_2^+$.

positive and the signal enhancement is called a positive signal. If the 396 nm pulse is before the 264 nm pulse the delay time is negative and the signal enhancement is called a negative signal. In the case of the I^+, CF_2I^+, and I_2^+ transients a positive signal is detected, in the case of $CF_2I_2^+$ and CF_2^+ a negative signal is observed. All transients were normalized to their maximum value. Around zero time delay the ion yield of I^+, CF_2I^+, and I_2^+ are comparable and 2–3 times larger than the parent ion peak. The ion yield of CF_2^+ is much smaller.

For most fragments the transients look very similar to the ones reported recently by Radloff and co-workers.[6] However, there appear to be some differences. First of all for the parent ion $CF_2I_2^+$ a small enhancement is observed at negative times. This means that a long-lived state must be accessed by multiphoton absorption of the pulse at 396 nm, followed by ionization of the 264 nm pulse. Perhaps this small channel is observed because we have a higher intensity of the 396 nm pulse than in the experiments of Radloff and co-workers. They report that typically they operated with fluences of about 1–10 mJ/cm^2 (pulse width about 130 fs) or even much smaller fluences of 40 μJ/cm^2 for the photoion–photoelectron coincidence experiments, where in our experiments the transients were taken with typically around

TABLE I. Fit parameters of the femtosecond pump–probe transients. In all the fits a constant crosscorrelation width σ=122 fs was used.

Fragment	Pump–probe time	Peakmax (fs)	t_0 (fs)	τ_1 (fs)	τ_2 (fs)	c
CF_2^+	neg	160	60	120	$\leqslant$250	0.01
$CF_2I_2^+$	neg	0	40	74	$\leqslant$250	0.04
I^+	pos	60	40	130	$\leqslant$250	0.09
I_2^+	pos	100	41	104	$\leqslant$250	0.02

60 mJ/cm^2 of the 396 laser pulse. The much higher fluences may facilitate weak multiphoton pathways accessible when the 396 nm pulse is before the 264 nm pulse. Another difference is that the maximum of the I_2^+ transient seems less shifted relative to the peak of the $CF_2I_2^+$ parent as compared to the experiment of Radloff and co-workers. The peak of the CF_2^+ transient appears to be shifted to positive time, in accordance with the observation of Radloff and co-workers. In our experiment we did not measure *in situ* an additional transient on a different molecule like benzene to determine accurately zero time delay. Perhaps around time zero, there is a small other pathway producing I_2^+, a multiphoton excitation of the 396 nm pulses first, followed by absorption of the 264 nm pulse. This weak channel may shift the peak of the I_2^+ transient closer to time-zero than is observed in the experiments of Radloff and co-workers. Also the very small CF_2^+ transient at negative times may be a signature of this small multiphoton pathway induced by absorption of the 396 nm pulse followed by absorption of the 264 nm pulse. This pathway appears to be absent at the much lower laser intensities used in Ref. 6. In Fig. 1 the energy level scheme of CF_2I_2 is shown. It can be seen that at the one pump (264 nm) photon level there is no stable state in which molecular iodine can be formed. This is in accordance with nanosecond experiments.[10] It means that only at short delay times photon schemes involving one 264 nm pump photon are possible to produce molecular I_2^+ photofragments. At longer times the CF_2I_2 molecule will have dissociated in a multibody decay to CF_2+I+I.

The transients of I_2^+ and I^+, which show a long time enhancement at positive delay times, were fitted with the following equation:

$$I(t)=\int_{-\infty}^{t}[e^{-(t'-t_0)/\tau_1}+c[1-e^{-(t'-t_0)/\tau_2}]] \times e^{-(t'-t)^2/2\sigma^2}H(t'-t_0)dt'. \quad (1)$$

In Eq. (1) the first term represents a fast exponentially decaying channel with a time constant τ_1. The second term represents an exponential rising channel with a time constant τ_2 and a weight given by the constant c. The width of the cross correlation of our experiment is given by σ. H represents the Heaviside function. In our fitting we have chosen a form similar to but simpler than the contributing transients reported by Radloff and co-workers.[6] The results of the best fit parameters are listed in Table I. In general the long term signal has a rather fast rise time τ_2. It turns out that with our cross correlation σ=122 fs (see Table I), we can at most

give an upperbound for the time constant τ_2. For $\tau_2 > 250$ fs we clearly see a deviation between the fitted and measured transients. Because we are only able to provide an upper limit for τ_2 we cannot unambiguously conclude that the fast decay ($\tau_1 \approx 100-130$ fs) of the initially excited state is to a state from which there is a long time formation of I_2^+ and I^+ possible. From our analysis we can only infer that the upper-limit of the fast build-up time τ_2 may be related to the fast initial decay τ_1 of the strong I_2^+ and I^+ signals.

For the transients of $CF_2I_2^+$, CF_2I^+, and CF_2^+ we used a similar expression as Eq. (1) with reversed positive and negative time.

Farmanara *et al.*[6] used three components to fit the pump-probe transients. They fitted the I_2^+ transient using two components at $\tau=0$, a contribution were one photon is absorbed from the pump laser directly followed by the absorption of two probe photons and a contribution in which one pump photon is absorbed and via fast ($\approx$30 fs) internal conversion another state is formed which is probe by absorption of two photons. At long delay times a two-photon contribution was fitted using an exponential rise. They found a small contribution for the ''direct'' one photon contribution around $\tau=0$. The velocity map images of our data (see Sec. III B) reveals two contributions around $\tau=0$. A contribution from an one photon transition of the pump laser and a contribution from a two-photon transition of the pump laser. The decaying state can be identified with the one photon transition being the *A* band of CF_2I_2. The weight of both contributions is approximately equal. This is different from the findings of Radloff and co-workers who attributed all the signal around $\tau=0$ to the one photon process. The ratio of the fluences between probe and pump is higher in our experiment, favoring the multiphoton contribution in our experiment. This fluence effect can also be seen in the fragment formation. Radloff *et al.* reported an identical shift of the peak maxima in the CF_2^+, I_2^+, and the I^+ transients.[18] We observed a shift of the peak maxima to longer times, indicating multiphoton contributions of the probe laser. A more detailed discussion of the contribution can be found below.

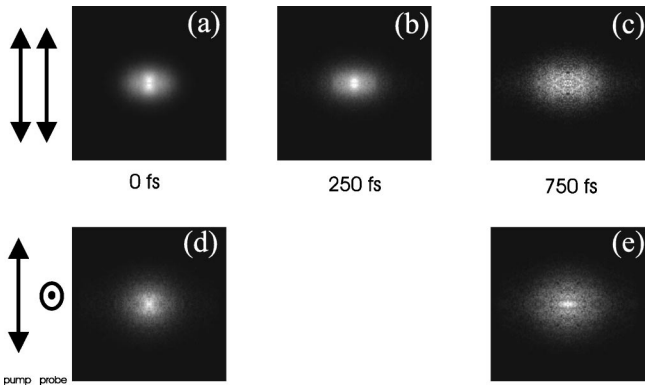

FIG. 3. Velocity map ion images of the I_2^+ fragment, for parallel pump–probe polarization configuration, at (a) 0 fs delay, (b) at 250 fs delay, (c) 750 fs delay. Similar, but for perpendicular pump–probe laser polarization configuration, (d) at 0 fs delay and (e) 750 fs.

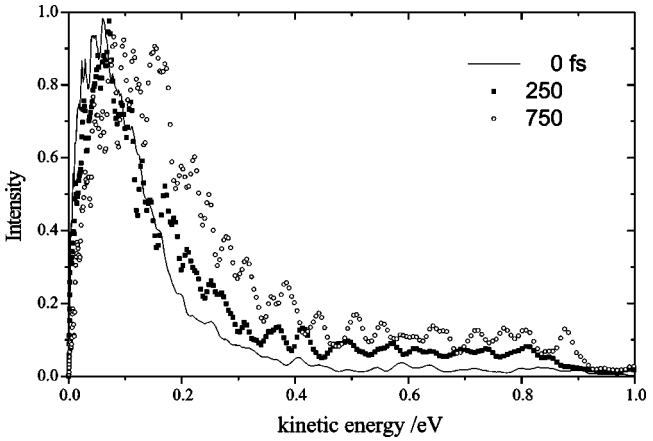

FIG. 4. Kinetic energy release of the I_2^+ fragment as a function of delay time.

B. Velocity map images

In the present study we have mostly concentrated on the molecular detachment channel of I_2^+ and most images reported here were measured for this channel. We did measure images also for the I^+, CF_2^+, and CF_2I^+ fragment channels. The average integration time used to record one image was typically about 4 min around time zero and up to about 20 min at long time delays where the signals are much weaker. In general, weak one laser signals were only observed from the 264 nm laser. To account for background signal from the 264 nm pump laser, at each delay an image was recorded with only the 264 nm laser and the 396 nm laser blocked. This background image was subtracted from the two laser image.

Velocity map images of I_2^+ are shown in Fig. 3, for parallel polarization at three delay times, 0 (a), 250 (b), and 750 fs (c) and for perpendicular polarization at 0 (d) and 1000 fs (e). In the center of these images, i.e., for I_2^+ fragments with low kinetic energy, a higher intensity is observed along the polarization of the lasers. This is typical of a recoil-distribution for a parallel transition. At larger distances away from the center, i.e., for I_2^+ fragments with higher kinetic energy, more intensity is observed at angles perpendicular to

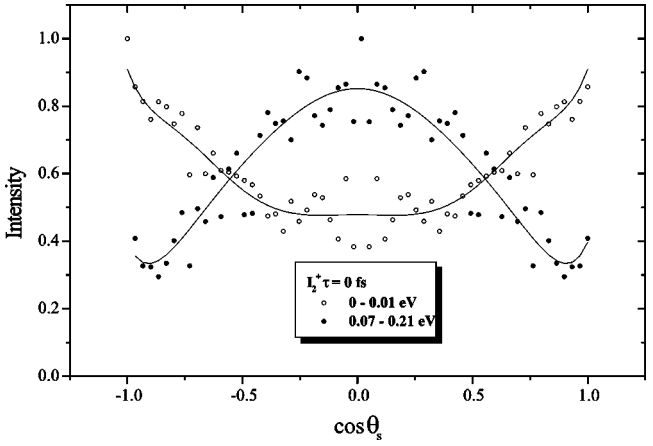

FIG. 5. The angular distributions of the I_2^+ fragment at 0 fs delay with ion kinetic energy in the energy ranges between 0–0.01 and 0.07–0.21 eV.

TABLE II. Angular distributions of the I_2^+ fragment. The first three rows are from Abel-inverted three-dimensional images with the polarization of the pump and probe laser parallel, the last two rows are from a direct fit to the two-dimensional experimental image with the polarizations perpendicular.

E_{kin} (eV)	0–0.01	0.01–0.07	0.07–0.21
τ (fs)	β, γ	β, γ	β, γ
0	0.5, 0.0	0.0, 0.1	−0.9, 0.3
250	0.2, 0.0	−0.2, 0.1	−0.9, 0.3
750	−0.3, 0.1	−0.1, 0.0	−0.4, 0.1
0	0.0, 0.0	0.0, 0.0	−0.3, 0.1
1000	−0.3, 0.0	−0.1, 0.0	−0.4, 0.1

the polarization, which is indicative of a more perpendicular transition. It seems that at larger delay times the channel with low kinetic energy disappears.

When the polarization of the 396 nm pulse and the 264 nm pulse are both parallel and in the plane of the detector the images have cylindrical symmetry. The images can be analyzed using the so-called inverse Abel-transform to obtain the original three-dimensional distribution.[17] By integrating the three-dimensional distribution at constant radii over the angular dimensions we obtain the kinetic energy distribution of the fragment. Figure 4 shows the kinetic energy distribution of the I_2^+ fragment as a function of delay time. A gradual shift towards higher kinetic energy can be observed.

By integrating the three-dimensional distribution over certain radii, corresponding to certain energy windows, we obtain the angular distribution of energy-selected fragments. In Fig. 5 the angular distribution is shown at zero delay time for I_2^+ fragments in two energy windows.

The angular distribution of the three-dimensionally inverted distribution was fitted to the following expression:[17]

$$I(\theta_s) = \frac{\sigma}{4\pi}[1 + \beta P_2(\cos\theta_s) + \gamma P_4(\cos\theta_s)]. \quad (2)$$

In Eq. (2) the parameters β and γ represent the anisotropy in the angular recoil distribution of the scattered photofragments, P_2 and P_4 represent the second and fourth Legendre polynomial and θ_s is the scattering angle between recoil velocity and pump laser polarization in the laboratory frame. The best fit parameters for I_2^+ are listed in Table II for fragments selected in three different energy ranges. Because the images for perpendicular polarization geometry cannot be inverted directly we have fitted Eq. (2) directly to the two-dimensional projected data.[17] The best fit parameters are also given in Table II. As can be seen in Table II, at 0 delay time,

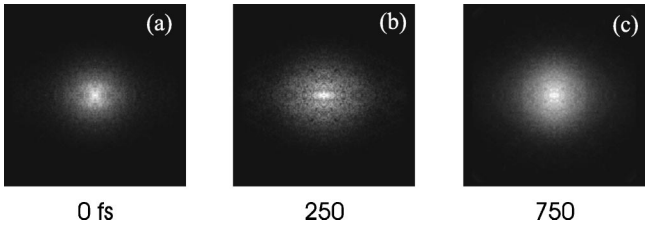

FIG. 6. Velocity map ion images of the I^+ fragment and parallel pump–probe laser polarization configuration, at delay times (a) 0, (b) 250, and (c) 750 fs.

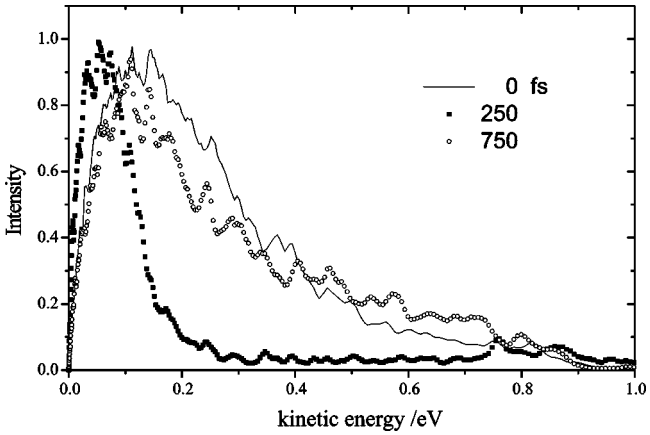

FIG. 7. Kinetic energy release of the I^+ fragment as a function of delay time.

and parallel polarization, a positive $\beta = 0.5$ for low kinetic energy, and a negative $\beta = -0.9$ at high kinetic energy is observed indicating a different mechanism responsible for molecular detachment of I_2^+.

The I^+ images are shown in Fig. 6 and were obtained for the parallel polarization configuration at three delay times, 0 (a), 250 (b), and 750 fs (c). These images exhibit an almost isotropic distribution. Figure 7 gives the kinetic energy distribution and Fig. 8 the angular distribution of the I^+ fragment.

Figure 9 shows the ion images for CF_2I^+ at 0 (a) and −670 fs (b) and the ion image of CF_2^+ at 0 fs (c), all three images were recorded for parallel polarization of pump and probe lasers. The ion image of CF_2^+ shows a perpendicular type of transition. We have summarized the angular distributions fitted to the data for I^+ in Table III, CF_2^+ in Table IV, and CF_2I^+ in Table V. In Sec. IV we will further discuss the angular and energy distributions obtained for the various fragments.

IV. DISCUSSION

A. The I_2^+ fragment

One of the main features observed in the velocity map images of the I_2^+ fragment is the strong parallel type feature

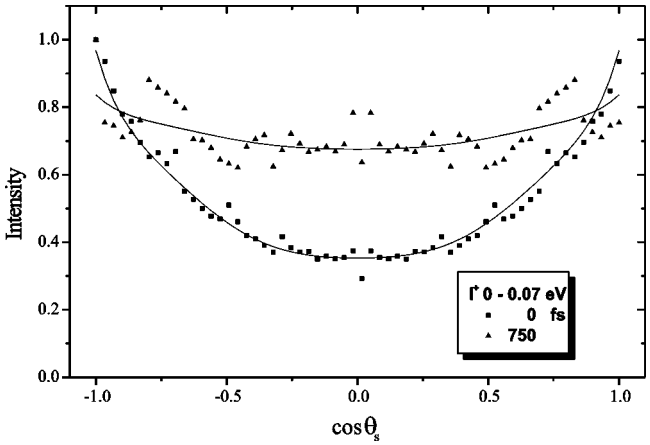

FIG. 8. Angular distribution of the I^+ fragment in the kinetic energy range between 0–0.07 eV at two delay times.

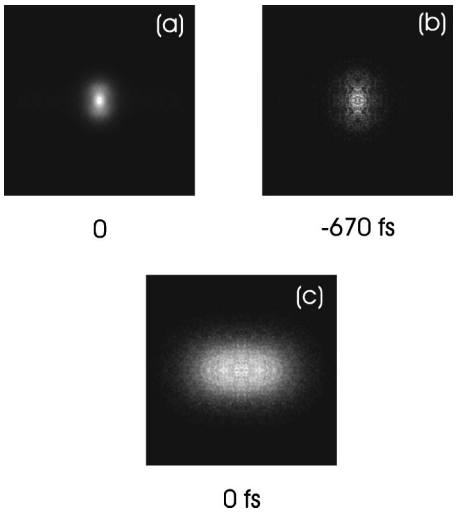

FIG. 9. Velocity map ion image of the CF_2I^+ fragment at (a) 0 fs delay and (b) -670 fs. (c) Velocity map ion image of the CF_2^+ fragment at 0 fs delay.

of slow fragments at short time delay, which disappears at longer times, and the more perpendicular feature of fast fragments, which is present also at longer times. In general, conservation of energy in the ionization and fragmentation processes dictates the following relation:

$$E_{\text{int,parent}} + nh\nu_1 + mh\nu_2 = E_{\text{diss}} + E_{\text{kin,frag}} + E_{\text{int,frag}} + E_{\text{electron}}. \quad (3)$$

In Eq. (3), $E_{\text{int,parent}}$ is the initial internal energy of the CF_2I_2 parent molecule, which in our cold seeded molecular beam is expected to be relatively low, so $E_{\text{int,parent}} \approx 0$. The number of absorbed pump photons with frequency ν_1 is given by n, the number of absorbed probe photons with frequency ν_2 is given by m. E_{diss} is the total energy needed to produce a particular dissociation channel with zero internal energy in the fragments. $E_{\text{kin,frag}}$ is the total kinetic energy produced in the dissociation and $E_{\text{int,frag}}$ is the total internal energy of the fragments. As is shown in Eq. (3), to obtain a complete characterization of the energetics, the kinetic energy of the ejected electrons, E_{electron}, is also needed. In the recent photoelectron–photoion coincidence study by Radloff and co-workers,[6] the photoelectron spectra in coincidence with I_2^+ were measured at zero time delay and at 1 ps delay. At 0 fs the distribution is rather broad, with no clear structure, and electron energies ranging up to about 1 eV are observed. At 1 ps pump–probe delay the photoelectron spectrum is quite different and dominated by a single peak at very low electron energies of about 0.1 eV. Radloff and co-workers conclude from their data that around zero delay and at short time delay the molecular I_2^+ fragment is formed by a $(1+2')$ absorption process, and a one-photon excitation by the pump laser followed by a two-photon excitation by the probe laser. They suggest that the two-photon excitation by the probe is mainly from an electronically excited state of the CF_2I_2 molecule reached by a very rapid internal conversion process within about 30 fs. The parent molecule in this electronically excited state subsequently dissociates rapidly in a three-body process to form the neutral products CF_2+I+I.

At long time delay of 1 ps, Radloff and co-workers report that the I_2^+ fragment is formed by absorption of two photons of the pump laser to an excited state of CF_2I_2, which very rapidly ($\leqslant 100$ fs) dissociates to CF_2 + electronically excited I_2. The excited I_2 can be ionized by absorption of one or two photons of the probe laser.

In the case of a two-body decay producing $CF_2+I_2^+$ the kinetic energy of the nonionized fragment can be calculated using conservation of momenta. The total photon energy of the $(2+1')$ excitation is 12.5 eV. The energy needed to produce the $CF_2+I_2^+$ channel is 10.5 eV. This means that at most about 2 eV of energy is available in total for kinetic energy and internal energy of the fragments when a slow electron of about 0.1 eV is formed. Using the conservation of momenta this leaves at most a fraction of $1/(1+m_{I_2}/m_{CF_2})$ of the available energy for kinetic energy of the molecular iodine fragment. This results in a cutoff energy of 0.3 eV, which agrees with what is observed for the maximum kinetic energy at long delay times (see Fig. 4). The peak of the kinetic energy distribution is observed around 0.1 eV. Using the photoelectron energy of 0.1 eV, this results in a sum of the internal energies of both the I_2^+ and CF_2 fragments of 1.2 eV. This energy is not sufficient to produce an electronically excited CF_2 fragment.[19]

A possible mechanism for the formation of an internally highly excited I_2^+ fragment may be the following. A two-photon absorption by the pump excites CF_2I_2 to a highly excited Rydberg state. The symmetry of this state, or an electronically excited state reached by internal conversion from the initially excited state, must be such that it has bonding electronic character along the I–I bond but repulsive charac-

TABLE III. Angular distributions of the I^+ fragment. The upper three rows are recorded in the parallel polarization geometry and the lower one in the perpendicular geometry.

E_{kin} (eV) τ (fs)	0–0.07 β, γ	0.07–0.2 β, γ	0.2–0.46 β, γ
0	0.7, 0.1	1.0, −0.1	1.2, 0.1
250	0.2, 0.2	−0.4, 0.2	⋯, ⋯
750	0.1, 0.0	0.1, 0.1	−0.3, 0.2
0	0.2, 0.0	0.4, 0.0	0.3, 0.0

TABLE IV. Angular distribution of CF_2^+ at $\tau = 0$ fs.

E_{kin} (eV)	β	γ
0–0.13	−0.1	0.1
0.13–0.38	−0.7	0.2
0.38–1.13	−1.0	0.4

TABLE V. Angular distribution of CF_2I^+.

E_{kin} (eV) τ (fs)	0–0.01 β, γ	0.01–0.05 β, γ	0.05–0.12 β, γ
0	0.2, 0.0	0.5, 0.0	0.8, 0.1
−670	0.3, 0.0	0.5, 0.1	0.8, 0.5

ter along the C–I coordinate. The molecule dissociates and the I_2 fragment is formed in a highly electronically excited state, for instance the $^2\Pi_{3/2}5d;2g$ state.[20] This Rydberg state couples vibronically with an ion pair state of I_2, which results in highly vibrationally excited molecular I_2, explaining the large amount of internal energy observed in the images. The formation of this ion pair state could be the mechanism via which the molecular iodine is detached from the molecule, which was also proposed by Dantus and co-workers for the similar system CH_2I_2.[5]

Besides the information on the energetics the images provide also the angular anisotropy of the recoiling fragments. We can extract the angular distribution for selected energy regions of the photofragments from the Abel-inverted three-dimensional image. In Fig. 5 the angular distribution at 0 fs is plotted for I_2^+ fragments with kinetic energy from 0 to 0.01 eV and 0.07 to 0.21 eV. The angular data suggests that in the low energy channel a different process is responsible for the formation of I_2^+ compared to the high energy channel. I_2^+ fragments with kinetic energy from 0 to 0.01 eV recoil in a more parallel distribution. As was discussed above, this channel disappears at longer delay time. The I_2^+ fragments with this low kinetic energy are most likely produced by a $(1+2')$ multiphoton excitation. Such a process is at the one-photon pump excitation resonant with the fast dissociative $^1B_1$ state[10] (see Fig. 1). If we assume that the one-photon step has 75% perpendicular character (note that there is some discussion in the recent literature[11] about the symmetry of the excited states around 4–5 eV), and the two-photon absorption by the probe laser has a 90% parallel character, we find in the limit of a fast axial recoil and no dynamics at the one-photon intermediate level[17] $\beta=0.5$ and $\gamma=0$. The experimentally observed (see Table II) are equal to these theoretical anisotropy values for this $(1+2')$ excitation assuming the above contributions of parallel and perpendicular character in the excitation steps.

For the I_2^+ fragments recoiling with energy in the higher energy channel from 0.07 to 0.21 eV the recoil distribution has a more perpendicular angular symmetry (see Fig. 5). As was discussed above, this more energetic channel is produced by a two-photon absorption by the pump laser. This transition is resonantly enhanced at the one-photon level by the A band which has $^1B_1$ symmetry. If we assume that the second absorption step of the pump photon is also a perpendicular transition, and we assume that the probe excitation is parallel, a $(2+1')$ process would lead to $\beta=-1.4$. We observe experimentally $\beta=-0.9$, see Table II.

Formation of highly excited molecular iodine on the two photon level is consistent with the angular distributions. Note that at delay times $\tau\geqslant 250$ fs the experimentally observed β and γ for the parallel configuration and the perpendicular configuration are identical (see Table II). Although the data recorded in the perpendicular configuration is a projected 2D-image, for the highest energy channel the β parameter is largely uneffected by the Abel-transform and the values obtained from the 2D-projected image resemble the value of the 3D-inverted image. From the similarity of the angular distribution for parallel and perpendicular polarization geometry we conclude that the dissociation already has taken place in about 250 fs. The probe photon is merely used to ionize the molecular Iodine. In order to ionize the molecular iodine with one probe photon of 396 nm, the molecular iodine has to have high internal energy (≈ 6.62 eV). For a $(2+1')$ photon scheme this gives 0.33 eV as a cutoff value for the kinetic energy of the molecular iodine fragment which is in accordance with the observed kinetic energy distribution (see Fig. 4).

The time reversed reaction of the molecular photodetachment of I_2 from CF_2 is the addition of a carbene to a single bond. This explains the special interest for the reactions $CX_2Y_2 \rightarrow CY_2 + X_2$. For these type of reactions it is known that the smaller the HOMO-LUMO gap in the expelled dihalogen, the smaller should be the reaction barrier and the degree of rotational excitation of the products.[1]

In case of an asynchronous detachment of the molecular iodine from CF_2I_2 the torque exerted may substantially lower the anisotropy in the angular distribution. That this may be the case can be concluded from the fact that the dissociation process is almost prompt ($\leqslant 250$ fs) but has a low anisotropy in the angular distribution, $\beta=0.5$, whereas the limiting cases for a $(2+1')$ process are $\beta=3.33$, for a pure parallel process, and $\beta=-1.67$ for a pure perpendicular process.[17] In case that the probe photon merely ionizes the products, $\tau\geqslant 250$ fs, the limiting values for a two photon transition are $\beta=2.86$ for purely parallel transitions and $\beta=-1.43$ for purely perpendicular transition.[17]

The rotation of the parent-ion molecule before dissociation can be neglected as a cause for the reduction of the anisotropy. The rotational constant of CF_2I_2 is estimated to be 0.0196 cm^{-1} from the values given in Ref. 21. Using this value we can estimate the most probable rotational state in a cold molecular beam of CF_2I_2 with a typical rotational temperature of about 10 K. This temperature would amount to rotational levels $J=13$ to be populated. The tangential velocity for the CF_2I_2 parent molecule can be calculated to be 0.5 m/s at the center-of-mass of the I_2. This value is only 1% of the radial velocity of the I_2^+ fragment, which for the low kinetic energy of 0.01 eV amounts to about 87 m/s. Additionally, due to the short dissociation time the parent rotation can be neglected.

We can estimate the reduction in the β parameter as follows. We first consider the effect of a finite lifetime and impulsive recoil on the reduction of the β-parameter, see also Fig. 10. The final recoiling fragments are CF_2 and I_2, and we use the model developed by Busch and Wilson[22] for a pseudodiatomic molecule XY (with $X=CF_2$, $Y=I_2$). Using the expressions developed for a dissociating molecule, we can calculate the reduction of the β-parameter using the following expression:[22]

$$\beta = \frac{P_2(\cos\alpha) + \psi^2 - 3\psi\sin\alpha\cos\alpha}{1+4\psi^2}\beta_{\text{impulsive}}. \qquad (4)$$

In Eq. (4) the following expressions are used: $\sin(\alpha) = \omega r/u$, $\mathbf{u}=\mathbf{u}_0+\mathbf{v}_t=\mathbf{u}_0+\omega\times\mathbf{r}$, $\psi=\omega\tau$. The various symbols have the following meaning: ω is the angular velocity; $\mathbf{u}$ is the recoil velocity; $\mathbf{u}_0$ is the radial recoil velocity; $\mathbf{v}_t$ is the tangential recoil velocity; τ is the (delay) time after initial

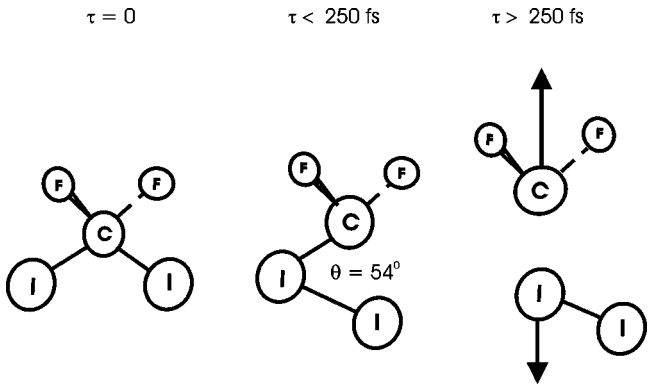

FIG. 10. Schematic of the asynchronous bondbreaking resulting in highly rotationally excited I_2. The angle θ is the CF_2–I–I angle at the moment the second bond breaks, and which is used to estimate the rotational excitation in an impulsive energy release model (Ref. 23). See also the text.

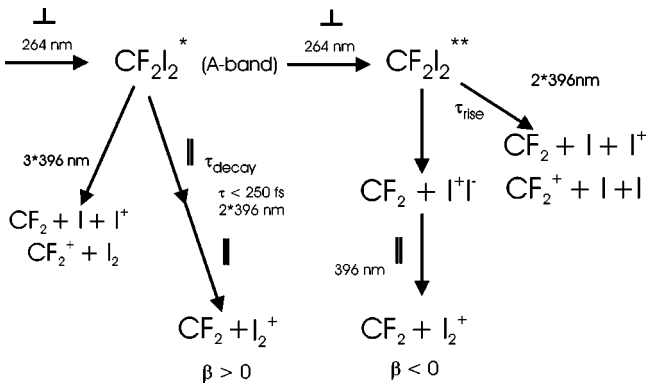

FIG. 11. Schematic overview of the events which occur in the photodissociation of CF_2I_2, adapted from Ref. 6.

excitation by the pump pulse. $\beta_{\text{impulsive}}$ is the β-parameter for an axial impulsive recoil with no dynamics, and $P_2(\cos\alpha) = \frac{3}{2}\cos^2\alpha - \frac{1}{2}$.

Solving Eq. (4) for fragments with kinetic energy in the energy interval 0.07–0.21 eV and using $u_{I_2} = 326$ m/s (corresponding to a kinetic energy of 0.14 eV from the experimental data) and $r_{I_2-CF_2} = 1.78$ Å, we obtain $\beta = -0.9$ for $\tau = 250$ fs and $\omega = 0.42 \times 10^{12}$ rad s^{-1}.

The calculated β-parameter using this simplified pseudodiatomic dissociation model is equal to the experimentally observed value when the angular velocity ω has the magnitude as given above. Furthermore, we can extent the analysis to account for the internal structure of the pseudodiatomic. We can use the impulsive recoil model[23] for pseudotriatomic molecules after the instantaneous bondbreaking of the first C–I bond and the rapid formation of the I–I bond, and the second asynchronous bondbreaking of the remaining C–I bond. Using this impulsive triatomic model we can calculate the rotational excitation, E_{rot}, in the recoiling I_2 molecule,

$$E_{\text{rot}} = E_{\text{excess}} \frac{m_I m_{CF_2} \sin^2\theta}{(m_I + m_I)(m_{CF_2} + m_I) - m_I m_{CF_2} \cos^2\theta}. \quad (5)$$

In Eq. (5) θ is the angle between CF_2–I–I when the second C–I bond breaks leading to impulsive rotational excitation in the I_2 molecule. E_{excess} is the total available energy which is estimated as follows: The two-pump photons have a total energy of 9.39 eV, the dissociation energy $D_{CF_2-I_2} = 1.2$ eV, and the electronic energy in I_2 is about 6.61 eV. This gives a maximum energy $E_{\text{excess}} = 1.57$ eV. Using a typical bond distance of I_2 of 3 Å (note that in the CF_2I_2 molecule[21] $r_{I-I} = 3.572$ Å and in the $^2\Pi_{3/2}5d;2g$ state of the free I_2 molecule $r_{I-I} \approx 2.6$ Å), the initial geometry of the CF_2I_2 molecule, and the slight rotation of the initial CF_2-I_2 axis due to the first bond rupture (estimated from the angular velocity ω after about 250 fs) of about 6°, we find from Eq. (5), $E_{\text{rot}} \approx 1200$ cm^{-1}. Using a rotational constant of I_2, $B \approx 0.030$ cm^{-1} (for $r \approx 3$ Å) we obtain $J \approx 200$. Of course, this calculation gives an estimate, and may be somewhat lower as some of the initial excess energy may be funneled into vibrational energy. The large rotational excitation is similar to the excitation observed for the molecular detachment of I_2 from CH_2I_2 which was also attributed to an asynchronous concerted elimination mechanism.[4]

B. The I^+, CF_2^+, and CF_2I^+ fragments

In this section we will discuss the various excitation processes which produce the other observed ionic fragment channels, I^+, CF_2^+, and CF_2I^+, see also Fig. 11.

We will first start with the formation of the I^+ fragment. Farmanara *et al.*[6] performed extensive photoion–photoelectron coincidence experiments, using different probe photon wavelengths of 400, 600, and 630 nm. To prevent false events the coincidence experiments were done with a substantially lower fluence of the probe laser, typically around 40μJ/cm^2. From the photoelectron spectra in coincidence with I^+, observed at a long pump–probe delay of 1 ps, they concluded that the iodine atoms are formed by dissociation of CF_2I_2 after absorption of three 267 nm pump photons. The dissociation leads to formation of neutral I atoms in highly excited Rydberg states, $6s$ and $6p$, see Fig. 1, after which only one 400 nm photon is needed to ionize these highly excited I atoms. This implies for the formation of I^+: $CF_2I_2 \rightarrow CF_2I + I^*(6p\ ^4P_{1/2})$, $D = 10.3$ eV.

In our experiments we excite with 264 nm pump photons and absorption of three 264 nm photons results in an excess energy of 3.8 eV for the dissociation to $CF_2I + I^*(6p\ ^4P_{1/2})$. Using the mass scaling factor 1/(1 +127/177), this gives an upper limit for the kinetic energy of the I atom of 2.2 eV, whereas from our imaging experiments we observe the peak in the kinetic energy distribution of the I^+ fragment around 0.2 eV (see Fig. 7).

It is not clear what causes the rather low kinetic energy of the I^+ fragment in our experiments. One possibility could be that a three photon pump excitation results in the formation of the neutral highly excited I atoms, with rather low kinetic energy of about 0.2 eV, and the formation of CF_2I fragments with a very high internal energy of around 3.5 eV. This may be somewhat unlikely. Another explanation may be that due to our much higher probe fluences (up to 60 mJ/cm^{-1}) we have a different pump–probe excitation process at longer delay times than observed in the experi-

ments by Radloff and co-workers using very low probe fluences. Figure 7 shows the kinetic energy distribution of the I^+ fragment at three different times. The pump–probe dependence is similar to the dependence observed for the I^+ fragment in the photodissociation of CF_3I.[17] In this latter experiment the lowering of the kinetic energy around $\tau=200$ fs was attributed to a $(1+3')$ process, whereas at $\tau=0$ and long delay times a $(2+2')$ process was observed.

We will now discuss the production of the I^+ fragment at longer delay times assuming a $(2+2')$ excitation. There are three possible schemes to produce the I^+ fragment:

(R1) $CF_2I_2 \rightarrow CF_2I_2^* \rightarrow CF_2I_2^{**} \rightarrow CF_2I + I^+$, $D=12.7$ eV,

(R2) $CF_2I_2 \rightarrow CF_2 + I_2^* \rightarrow CF_2 + I + I^+$, $D=13.2$ eV,

(R3) $CF_2I_2 \rightarrow CF_2I^* + I \rightarrow CF_2 + I^+ + I$, $D=13.2$ eV.

In the above reaction schemes the appearance energy D for the particular reaction is given. For reaction (R1) two intermediate electronically excited states are indicated as was suggested by Radloff and coworkers.[6] When a $(2+2')$ photon scheme is assumed, (R1) will have an excess energy of 3.0 eV available for the two fragments. We do not know what the electron energy is for such a $(2+2')$ photon scheme. If we use a similar electron energy of about 0.9 eV and subtract this from the excess energy we have 2.1 eV for total kinetic energy and internal energy of the CF_2I+I^+ fragments. Using the mass scaling factor this results in a cutoff kinetic energy of 1.2 eV for the I^+ fragment. In the energy distribution of I^+ (see Fig. 7) the highest values observed for I^+ are around 0.5–0.6 eV. This means the CF_2I fragment must be produced with an internal energy of about 1.1 eV which is quite high. In the case of a $(1+3')$ photon excitation scheme the second intermediate state does not exist, the excess energy for (R1) is 1.4 eV, and we obtain a kinetic energy cutoff of about 0.3 eV for the I^+ fragment.

The energetics for reaction (R2) cannot be calculated directly, as we have a sequential dissociation, first into $CF_2+I_2^*$, followed by ionization and dissociation of I_2^* to $I+I^+$. If we assume again that the first dissociation is from a two-photon absorption of 264 nm (9.36 eV total photon energy) and the dissociation energy of CF_2+I_2, $D=1.2$ eV, we have 8.26 eV available for internal and recoil energy of $CF_2+I_2^*$. We have observed that it is possible that one 396 nm probe photon ionizes to form I_2^+. Using the ionization energy of I_2 (9.30 eV) it means that the internal (mostly electronic) excitation of I_2^* has a lower bound of 6.2 eV. If we subtract this from the available energy and scaling with the mass-factor for CF_2+I_2, we find that the maximum kinetic energy of I_2^* is 0.34 eV. Excitation of the internally highly excited I_2^* fragments with two probe photons of 396 nm (6.26 eV), and subtracting the dissociation energy of I_2 (1.542 eV) and the ionization energy of I (total of 9.307 eV) we find $6.2+6.26-1.542-9.307=1.61$ eV available for electron energy and kinetic energy. If we assume again that the electron takes away about 0.9 eV we obtain a kinetic energy from $I_2^* \rightarrow I+I$, of 0.36 eV. This means that for the total process the I^+ may recoil with at most $0.36+0.34=0.7$ eV.

Reaction (R3) is energetically unlikely, the appearance energy for the first step is 2.2 eV which gives after the absorption of two 264 nm photons an $E_{\text{cutoff}}=4.2$ eV for the kinetic energy of the iodine atom, which is not observed. Also no long term enhancement with 264 nm as pump is observed in the CF_2I^+ transient, making a highly internally exited CF_2I fragment unlikely. In the case of a $(1+3')$ photon process, three 396 nm photon have an energy of 9.4 eV, whereas the ionization energy of an iodine atom is 10.5 eV, which makes this pathway impossible.

Taking the above discussion into account we conclude that for our pump–probe fluences reaction (R2) is the most likely candidate for production of I^+ fragments. The shift to lower kinetic energies around $\tau=250$ fs, may be explained by assuming a $(1+3')$ excitation scheme at these intermediate times. Such an excitation gives an excess energy of 0.9 eV and a cutoff energy of the iodine atom of only 0.14 eV. Such a switch in the excitation scheme was observed in the multiphoton dynamics in CF_3I (Ref. 17) and may also explain the change observed in the CF_2I_2 dissociation dynamics for the I^+ fragment.

The angular distribution of the I^+ fragment with kinetic energy below 0.07 eV is shown in Fig. 8 for two delay times. The extracted anisotropy parameters for three different energy ranges are given in Table III. The anisotropy of the lowest kinetic energy channel is similar to the lowest I_2 channel at 0 and 250 fs delay. In the energy range from 0.07 to 0.2 eV at 250 fs delay the anisotropy parameter $\beta=-0.4$. This negative β-parameter supports a $(1+3')$ REMPI transition where the one-photon transition to the A-band has a perpendicular symmetry. The $(3+1')$ photon scheme proposed by Farmanara *et al.*[6] gives a total internal energy of about 2.5 eV for all fragments and seems less likely.

Next we turn to the multiphoton schemes leading to the CF_2^+ fragment. The formation of CF_2^+ can occur via two different pathways:

(R4) $CF_2I_2 \rightarrow CF_2^+ + I_2$, $D=12.62$ eV,

(R5) $CF_2I_2 \rightarrow CF_2^+ + I + I$, $D=14.2$ eV.

A $(2+2')$ photon pathway as well as a $(1+3')$ pathway have enough energy to produce fragments via reaction (R4). The excess energy of the $(2+2')$ is 3 eV, which leads to a cutoff in kinetic energy of the CF_2^+ fragment of 2.5 eV. Such high kinetic energy fragments are not observed. The $(1+3')$ photon pathway leads to a cutoff in kinetic energy of 1.2 eV, making this the most likely pathway for CF_2^+. This also explains why no long term positive signal is observed. The reaction (R5) is only accessible via the $(2+2')$ photon pathway, giving a excess energy of 1.4 eV. This fragment has an enhancement at negative pump–probe delay which means it is produced by a $(2'+2)$ photon pathway. This negative signal is also found in the production of the parent-ion, for which the photoion photoelectron coincidence measurements suggest it is a $(2'+1)$ photon process.[6] The negative time delay signal of the CF_2^+ fragment can be compared to the state excited by Scheld *et al.*[11] The angular data of CF_2^+ is more in favor of a two photon 264 nm at $\tau=0$ because of the negative β parameters. This negative parameter is most likely caused by a sequential absorption of two 264 nm photons both in a perpendicular transition. It is highly unlikely that this negative β parameter is caused by the two photon

transition of 396 nm while at 396 nm there is no resonance in CF_2I_2.

Finally, we discuss the production of the CF_2I^+ fragment which is only observed around zero delay time, similar to the results of Radloff and co-workers.[6] They attributed the formation of the CF_2I^+ ion to fragmentation of the parent $CF_2I_2^+$ ion after a $(1+2')$ or $(1+3')$ photon process. The production of CF_2I^+ fragments has a threshold of 10.3 eV, this means that in the case of a $(1+2')$ photon process (total photon energy of 10.96 eV), the excess energy is 0.66 eV. This corresponds to a cutoff energy of 0.28 eV for the kinetic energy of the CF_2I^+ fragment and is in accordance with the experimental kinetic energy distribution which we observed (not shown here). The electron kinetic energy distribution observed in coincidence[6] shows several peaks, two strong peaks around 0.1 and 0.4 eV, a somewhat smaller peak at 0.9 eV and a declining tail up to about 2 eV. It was concluded that all these peaks correlate with two-photon probe ionization from different electronic states in the CF_2I_2 molecule, and subsequent direct fragmentation into CF_2I^+ and I, or absorption of a third probe photon by $CF_2I_2^+$ followed by fragmentation. The kinetic energy distribution of the CF_2I^+ fragment shows a maximum at 0.06 eV which means a total kinetic energy of about 0.1 eV. The two stronger peaks at 0.1 and 0.4 eV are probably from the $(1+2')$ excitation which leaves at most 0.32–0.15 eV available for kinetic energy of CF_2I^+. The higher electron peak at 0.9 eV and the tail to 2.0 eV are probably due to $(1+3')$ excitation, possible also leading to formation of spin–orbit excited I-atoms, some internal energy of the CF_2I^+ fragment and low kinetic energy of the fragments. In general, the kinetic energy observed for the CF_2I^+ fragment is in agreement with the observations and conclusions of Radloff and co-workers.

V. CONCLUSIONS

In this study we have reported femtosecond time-resolved velocity map ion imaging experiments on the photodissociation and ionization of CF_2I_2. The velocity map imaging enables the measurement of the kinetic energy of the detected fragment, and as such correlates the remainder of the available energy with the internal energy of the cofragment and the kinetic energy of the electron. We have observed two distinct pathways leading to the detachment of molecular I_2^+. Up to a pump–probe delay of about 250 fs both pathways are active in the formation of molecular iodine. The $(1+2')$ pathway results in low kinetic energy I_2^+ with low internal energy. The recoil anisotropy reveals a parallel type of excitation symmetry. The $(2+1')$ pathway results in internally excited molecular Iodine and is observed even at long delay times up to 1 ps. The $(2+1')$ photon pathway may be via a state correlating to an ion-pair state located at the iodine molecule. This pathway produces rotationally hot I_2, $J=238$, which implies an asynchronous concerted mechanism of formation. The formation of I^+ is mostly via the same photon pathways, differing only in the absorption of one extra probe photon. Both the I_2^+ and I^+ fragment have an enhancement when the 396 nm beam is delayed relative to the 264 nm beam positive. The CF_2^+ fragment shows a negative signal, at $\tau=0$ the signal is mainly produced by a $(2+2')$ photon pathway which is in a positive time ordering. The CF_2I^+ fragment also has a very small long term enhancement at negative time delay. Also at $\tau=0$ the negative time signal contributes the most as can be derived from the positive values for the β parameters. Energetic correlations from imaging experiments provide very valuable insight into the mechanism and correlations of complex multiphoton excitation pathways. In the near future we will extend the imaging apparatus to incorporate coincidence imaging of photoelectron and photoion,[24] and as such the complete energetics of angular distribution of recoiling fragments can be determined. First application of this technique to study the multiphoton dynamics of CF_3 I were reported recently.[25]

ACKNOWLEDGMENTS

The research has been financially supported by the councils for Chemical Sciences and Physical Sciences of the Netherlands Organization for Scientific Research (CW-NWO, FOM-NWO). W.G.R. gratefully acknowledges CW-NWO for a Ph.D. fellowship within the Young Chemist Program. Mr. R. Mooyman provided excellent technical assistance in the day-to-day operation of the facilities in our femtolab. Mr. W. Feijen, Mr. J. van Stralen, and Mr. J. Buijs are gratefully acknowledged for their help in implementing various parts of the data acquisition and analysis software. The authors would like to thank Professor S. Stolte for his generous support. The authors acknowledge valuable discussions with Professor W. Radloff.

[1] S. R. Cain, R. Hoffmann, and E. R. Grant, J. Phys. Chem. **85**, 4046 (1981).
[2] F. Battin-Leclerc, A. P. Smith, G. D. Hayman, and T. Murrells, J. Chem. Soc., Faraday Trans. **92**, 3305 (1996).
[3] A. H. Zewail, J. Phys. Chem. A **104**, 5660 (2000).
[4] Q. Zhang, U. Marvet, and M. Dantus, J. Chem. Phys. **109**, 4428 (1998).
[5] U. Marvet, E. J. Brown, and M. Dantus, Phys. Chem. Chem. Phys. **2**, 885 (2000).
[6] P. Farmanara, V. Stert, H.-H. Ritze, and W. Radloff, J. Chem. Phys. **113**, 1705 (2000).
[7] M. Dantus, M. H. M. Janssen, and A. H. Zewail, Chem. Phys. Lett. **181**, 281 (1991); M. H. M. Janssen, M. Dantus, H. Guo, and A. H. Zewail, *ibid.* **214**, 281 (1993).
[8] E. A. J. Wannenmacher, P. Felder, and J. R. Huber, J. Chem. Phys. **95**, 986 (1991).
[9] G. Baum, P. Felder, and J. R. Huber, J. Chem. Phys. **98**, 1999 (1993).
[10] K. Bergmann, R. T. Carter, G. E. Hall, and J. R. Huber, J. Chem. Phys. **109**, 474 (1998).
[11] H. A. Scheld, A. Furlan, and J. R. Huber, Chem. Phys. Lett. **326**, 366 (2000).
[12] X. Zheng and D. L. Phillips, Chem. Phys. Lett. **316**, 524 (2000).
[13] M. S. Park, T. K. Kim, S.-H. Lee, K-H. Jung, H. R. Volpp, and J. Wolfrum, J. Phys. Chem. **105**, 5606 (2001).
[14] D. W. Chandler and P. L. Houston, J. Chem. Phys. **87**, 1445 (1987).
[15] A. T. J. B. Eppink and D. H. Parker, Rev. Sci. Instrum. **68**, 3477 (1997).
[16] W. G. Roeterdink and M. H. M. Janssen, Chem. Phys. Lett. **345**, 72 (2001).
[17] W. G. Roeterdink and M. H. M. Janssen, Phys. Chem. Chem. Phys. **4**, 601 (2002).
[18] W. Radloff, P. Farmanara, V. Stert, E. Schreiber, and J. R. Huber, Chem. Phys. Lett. **291**, 173 (1998).
[19] T. K. Minton, P. Felder, R. C. Scales, and J. R. Huber, Chem. Phys. Lett. **164**, 113 (1989).
[20] K. P. Lawley, T. Ridley, Z. Min, M. S. N. Al-Kahali, and R. J. Donovan, Chem. Phys. **197**, 37 (1995).

[21] H.-G. Mack, H. Oberhammer, E. O. John, R. L. Kirchmeier, and J. Shreeve, J. Mol. Struct. **150**, 103 (1991).
[22] G. E. Busch and K. R. Wilson, J. Chem. Phys. **56**, 3638 (1972).
[23] R. Schinke, *Photodissociation Dynamics* (Cambridge University Press, Cambridge, 1995).
[24] J. A. Davies, J. E. Leclaire, R. E. Continetti, and C. C. Hayden, J. Chem. Phys. **111**, 1 (1999).
[25] A. M. Rijs, C. C. Hayden, and M. H. M. Janssen, in *Femtochemistry and Femtobiology: Ultrafast Dynamics in Molecular Science*, edited by A. Douhal and J. Santamaria (World Scientific, Singapore, 2002), p. 91.